Determination of the potential for fundamental- and adjoint-representation sources in SU(2) in three dimensions

Robert D. Mawhinney
Department of Physics and Astronomy, University of Pittsburgh, Pittsburgh, Pennsylvania 15260
(Received 27 December 1989)

Pure SU(2) lattice gauge theory in three dimensions is studied by Monte Carlo simulation with a determination of the potential between fundamental- and adjoint-representation sources as a major goal. A 32^3 lattice is used and Wilson loops up to 16 by 16 are measured using a modification to the standard multihit variance reduction which improves the statistics by at least a factor of 3 at $\beta=6.0$. The integrated autocorrelation times measured for the loops show a peak for loops of size β by β. The fundamental- and adjoint-representation potentials are seen to have the same functional form to very high accuracy and their numerical values are in the ratio of their Casimir operators. The string tension is extracted and scaling is seen to within a few percent over a range of couplings which correspond to a factor of 2 change in the glueball mass. Correlated errors have been taken into account in the extraction of the potentials from the Wilson-loop values.

I. INTRODUCTION

Non-Abelian gauge theories have been investigated primarily through continuum perturbation theory, expansions around semiclassical solutions of the field equations, and both analytical and numerical analysis in the Euclidean lattice formulation. Gauge theories in different numbers of space-time dimensions have also been explored. Although no proof exists, it was widely expected and is now supported by data from numerical simulations[1-3] that non-Abelian gauge theories in both three and four space-time dimensions are confining theories with a mass gap.

In spite of the numerical evidence, no satisfactory explanation has yet been given for why these theories exhibit this behavior. Many of the attempts to understand the mechanisms responsible for producing confinement and a mass gap have focused on the SU(2) model in three Euclidean dimensions[4] [denoted by $SU(2)_3$ in this paper]. It is hoped that this model may be easier to understand than the four-dimensional version since it is superrenormalizable, with a dimensionful coupling constant.

Existing numerical studies for $SU(2)_3$ have given strong evidence for both a string tension[2] and a mass gap.[3] However, the studies that measured the string tension and parameters of the potential were all done using the icosahedral subgroup of SU(2), which restricted them from probing too far into the weak-coupling region, due to the freezing of the icosahedral subgroup.

Because of the usefulness of $SU(2)_3$ in efforts to understand the nonperturbative physics of non-Abelian gauge theories, an updated numerical simulation of this model is warranted. The purpose of this paper is to provide such a simulation, with the determination of the potential and string tension as the main goal. Because of the computing power now available, we can work at weaker couplings and with larger lattices than have been previously studied. Now standard variance reduction techniques are incorporated along with a modification which further reduces the variance. We can check for asymptotic scaling at weaker couplings than previously used. (Given the difficulty in observing scaling in four dimensions consistent with the two-loop beta function it is interesting to check the accuracy of scaling in this simpler model.) We have not devoted much effort to measuring the mass gap, and have no results to report on this.

In this study we work with the $SU(2)_3$ model on a cubic lattice with periodic boundary conditions. A configuration of the system is given by specifying an SU(2) matrix for each link of the lattice. The partition function is

$$Z=\int [dU]\exp(\beta S) , \tag{1}$$

where $[dU]$ is the product over all links on the lattice of the Haar measure for each link,

$$S=\frac{1}{2}\sum_p \mathrm{Tr}\prod_{l\in p} U_l , \tag{2}$$

and β is related to the continuum coupling constant g^2 by

$$\beta=1/2g^2a, \quad \beta\gg 1 , \tag{3}$$

where a is the lattice spacing.

The Wilson loop is defined for any closed loop L and any representation j by

$$W_j=(1/N)\mathrm{Tr}\left[\prod_{l\in L} D_j(U_l)\right] , \tag{4}$$

where $D_j(U)$ is an irreducible representation of the gauge group and N is the trace of the identity in that representation. As is well known the potential between an infinitely massive quark-antiquark pair, which transform according to the representation j, is given by

$$V_j(R)=-\lim_{T\to\infty}\frac{\ln W_j(R,t)}{T} , \tag{5}$$

where the Wilson loop is defined on a rectangular path of dimensions R by T. Since the expected (at least in the fundamental representation) linear potential means the Wilson loop behaves as $\exp(-\sigma_j RT)$ (σ_j is the string tension for representation j) for large R and T, it is also convenient to discuss the behavior of the Cruetz ratio, defined by

$$C_j(R,T)=-\ln\frac{W_j(R,T)W_j(R-1,T-1)}{W_j(R-1,T)W_j(R,T-1)} . \tag{6}$$

For large R and T, the Creutz ratio gives the string tension, if there is one. Because the coupling constant has dimensions, the string tension should scale as $1/\beta^2$ for weak coupling (large β).

Section II explains how additional variance reduction can be achieved in addition to the standard multihit variance reduction commonly used in gauge theories. Section III is devoted to a discussion of the details of the simulation. Section IV contains information about how the errors were handled, Sec. V gives the final results and Sec. VI contains the summary and conclusions.

II. VARIANCE REDUCTION

As is well known, it is advantageous in numerical simulations to be able to replace an observable with another quantity which averages to the same value as the original, but which has a smaller variance.[5] In the case of lattice gauge theory the usual choice when the observable is a Wilson or Polyakov loop is to replace each link U_l in the loop by

$$U_l\rightarrow\frac{\int dU_l\exp(\beta k_l \mathrm{Tr}U_l/2)U_l V_l^{-1}}{\int dU_l\exp(\beta k_l \mathrm{Tr}U_l/2)} , \tag{7}$$

where $k_l V_l$ is the sum of the staples which, with U_l, form plaquettes and k_l is a positive number determined by the condition that V_l be an SU(2) matrix. For SU(2) the integral can be done to give

$$U_l\rightarrow\frac{I_2(\beta k_l)}{I_1(\beta k_l)}V_l^{-1} . \tag{8}$$

For large β, k_l becomes very close to the number of staples which, with U_l, form plaquettes (four in three dimensions). Using the asymptotic expansions for the Bessel functions gives

$$U_l\rightarrow(1-3/8\beta+\cdots)V_l^{-1} . \tag{9}$$

Whereas the original quantity could take values between ±1, the new quantity takes values between $\pm(1-3/8\beta+\cdots)$.

In this work we have extended this idea to add a second variance reduction step in each link. To see how this is done, consider Fig. 1. It shows the four primary plaquettes containing U_l as well as 12 secondary plaquettes which border the initial four. To make the derivation transparent, we have chosen a gauge where the matrices on all links without arrows have been set to unity. The expectation value of an observable containing U_l

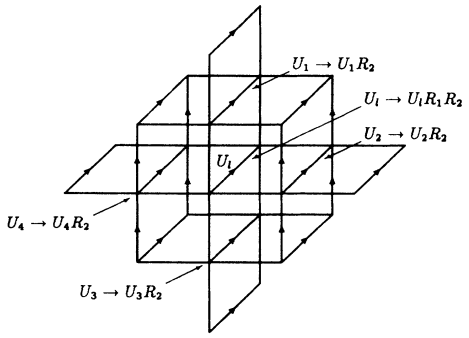

FIG. 1. The configuration used in deriving the double variance reduction [showing the substitution of Eqs. (11) and (12)].

is of the form

$$\langle O\rangle=\frac{1}{Z}\int[dU]\exp(\beta S)\mathrm{Tr}(U_l X) . \tag{10}$$

Make the substitution

$$U_l\rightarrow U_lR_1R_2 , \tag{11}$$

$$U_i\rightarrow U_iR_2,\quad i=1,4 \tag{12}$$

in (10), where R_1 and R_2 are arbitrary SU(2) matrices. Using the invariance of the Haar measure, integrating over R_1 and R_2 and dividing by two factors of the group volume v gives

$$\langle O\rangle=\frac{1}{Zv^2}\int[dU]\exp(\beta S')\int dR_1dR_2\exp(\beta S'')\times\mathrm{Tr}(U_lR_1R_2X) , \tag{13}$$

where S'' is the contribution to the action of all plaquettes drawn in Fig. 1 and S' is the contribution from all other plaquettes in the lattice. The integrals over R_1 and R_2 are decoupled and are easily done to give

$$\langle O\rangle=\frac{1}{Zv^2}\int[dU]\exp(\beta S')I_2(\beta k_1)I_2(\beta k_2)\times\mathrm{Tr}(V_1^{-1}V_2^{-1}X) , \tag{14}$$

where

$$k_1V_1=U_1+U_2+U_3+U_4 , \tag{15}$$

$$k_2V_2=T_1+T_2+T_3+T_4 . \tag{16}$$

T_i is the sum of the three staples connected to U_i which do not contain U_l. k_1 and k_2 are determined by the requirements that they are positive and V_1 and V_2 are SU(2) matrices. Note that the k's and V's are independent of U_l.

In (14) insert into the integrand the factor

$$1=\frac{\int dR_1dR_2\exp(\beta S'')}{I_1(\beta k_1)I_2(\beta k_2)} . \tag{17}$$

Using the inverse of the transformation given by (11) and (12) and then doing the trivial integrals over R_1 and R_2

gives

$$\langle O \rangle = \frac{1}{Z} \int [dU] \exp(\beta S) \frac{I_2(\beta k_1) I_2(\beta k_2)}{I_1(\beta k_1) I_1(\beta k_2)} \times \mathrm{Tr}(V_1^{-1} V_2^{-1} X) . \quad (18)$$

For large β, $k_1 \sim 4$ and $k_2 \sim 12$ so the ratio of the Bessel functions becomes

$$(1-3/8\beta+\cdots)(1-3/24\beta+\cdots) . \quad (19)$$

The second variance reduction reduces the variance by roughly the cube root of the amount that the initial reduction does.

Repeating the analysis above with the Wilson loop in the adjoint representation changes (18) to

$$\langle O_A \rangle = \frac{1}{Z} \int [dU] \exp(\beta S) f_1 f_2 \mathrm{Tr} D_A(V_1^{-1} V_2^{-1} X), \quad (20)$$

where

$$f_i = 1 - \frac{4}{\beta k_i} \frac{I_2(\beta k_i)}{I_1(\beta k_i)} \rightarrow 1 - 4/\beta k_i + \cdots \quad (\beta k_i \gg 1) . \quad (21)$$

Here we also see that the second variance reduction reduces the variance by the cube root of the first, although since the first is larger for the adjoint representation than the fundamental, the second is also larger. In Sec. IV we will check these estimates and discuss the usefulness of this addition.

III. THE SIMULATION

The simulation was done on a 32^3 lattice with periodic boundary conditions. A standard heat-bath algorithm was used to do the updating. All Wilson loops smaller than 16 by 16 were measured, except for adjoint loops at $\beta = 6.0$. Here the largest loops are too small to measure accurately, so no time was spent on them. All loops with one dimension greater than or equal to four were measured using the double variance reduction described in Sec. II, while the loops with one dimension less than or equal to four (except the single plaquette) were measured using single variance reduction. Since loops with one dimension equal to four were measured both ways, the effect of the second variance reduction can be determined.

For a single lattice, before measuring the loops, the necessary reduced variables (the V's and ratios of Bessel functions) were calculated for all links in the lattice. The calculation was organized so that all the staples calculated for the first variance reduction were used in calculating the reduced variables for the second variance reduction. In this way a lattice of singly reduced variables and a lattice of doubly reduced variables was produced. If the comparison between the single and double variance reduction were not of interest, all small loops could be measured on an unreduced lattice and only the doubly reduced lattice would need to be generated. Since each lattice is of size 0.4 megawords, for this problem both the singly and doubly reduced lattices could be kept (along with the original). (To reduce charges for fast memory usage, they were actually kept on the solid-state storage device of the Cray-XMP and were read in plane by plane when needed.)

Loops were measured in both lattices of reduced variables; small loops in the singly reduced lattice, large loops in the doubly reduced lattice. To measure loops, a plane was chosen and all links in one direction in that plane were gauged to unity. The links in the other direction were appropriately modified by multiplying with links from the unreduced lattice so that when all the parallel transporters were collected to form a loop, unreduced variables were used in the corners of the loops. (The derivation in Sec. II assumed that the R integrals are decoupled for neighboring links, which is true except near the corners).

Three values of β were used in this study: 6.0, 10.0, and 12.0. Previous studies have used values as large as 6.5 and found scaling at the 10% level for the string tension. [These β values are well above the crossover from strong to weak coupling which occurs for $\beta \sim 2.5$ (Ref. 6).] Table I shows the number of sweeps for each lattice. One sweep of the lattice took about 0.8 sec and one measurement of all loops on the lattice using the double variance reduction took about 9.5 sec. (Of this 9.5 sec, slightly less than 1 sec was needed to calculate the reduced variables for the secondary variance reduction from the already calculated quantities used in the primary variance reduction.) Initially measurements were performed only on fundamental representation loops.

During the 1000 sweeps shown in the autocorrelation column all square loops were measured after each sweep so that an estimate of the autocorrelation time could be used to determine a reasonable separation between measurements (given in the last column of Table I). For an observable O, whose average is obtained from a time series, the integrated autocorrelation time is found as follows. (See Ref. 7, and references therein for a more detailed derivation.) Define the correlation function for an observable O as

$$\rho(t) = \frac{\sum_i [O(i)-\bar{O}][O(i+t)-\bar{O}]}{\sum_i [O(i)-\bar{O}][O(i)-\bar{O}]} , \quad (22)$$

where the sums are over all measurements and $\bar{O}$ is the average value of O. The integrated autocorrelation time is found by summing $\rho(t)$ over t and equating this value with the sum over t of $\exp(-|t|/\tau_{\mathrm{int}})$. The sum over t of $\rho(t)$ must be cut off at some value to keep the poor statistics in the tail of $\rho(t)$ from making the answer meaningless. (The cutoff used is discussed in Sec. IV.)

Table II gives the integrated autocorrelation times for square loops. For each value of β, two autocorrelation times are shown. The preliminary estimate based on 1000 measurements is shown in the column marked initial. These times were used only to help determine the number of sweeps between measurements given in Table I. The column marked final is based on all the measurements of the loops, where the separation between mea-

TABLE I. The number of sweeps and measurements used in the simulation.

β	Thermalization	Sweeps used for Autocorrelation	Measurement Fundamental	Measurement Adjoint	Separation
6.0	5600	1000	5000	2000	10
10.0	7700	1000	3000	1000	20
12.0	10200	1000	2500	500	20

surements is given in Table I. The errors on the times in the column marked final are between 5 and 10% [found through formulas similar to (27)], while the times in the initial column are rough estimates due to the limited number of sweeps involved. For $\beta=10.0$ the initial estimate is much larger than the final result. To check that this was just the result of poor statistics in the initial estimate, the measurements used to calculate the final result were broken into small groups of the same size as the initial measurement and the groups displayed sufficient variance to account for the largeness of the initial estimate. An interesting feature of the autocorrelation times is that they peak for loops of size very near β by β.

IV. STATISTICAL CONSIDERATIONS

Since this work is motivated by the goal of providing an accurate determination of the potential for this model, particular care has been taken in the statistical analysis of the data. For two observables X and Y, both simultaneously measured from the same sequence of lattice configurations, the full covariance matrix can be estimated from the measured values. The estimate for the covariance matrix is found by first calculating

$$\xi_{XY}(t)=\frac{1}{N}\sum_i \hat{X}(t+i)\hat{Y}(i) \tag{23}$$

for the data sample where

$$\hat{X}(i)=X(i)-\bar{X} , \tag{24}$$

N is the number of measurements, and $\bar{X}$ is the sample mean. [The sum in (23) is actually over at most $N-t$ measurements, where the normalization is also changed appropriately. We will use the simple notation of (23) for convenience.] The covariance matrix is then given by

$$C_{XY}=\frac{1}{N}\sum_{-T_c}^{T_c}\xi_{XY}(t) , \tag{25}$$

where T_c is a cutoff that must be determined. If T_c is taken as large as allowed by the number of measurements, it can be shown that the variance of the estimate for the covariance matrix does not go to zero as the number of measurements of the observables goes to infinity.[7] Taking T_c smaller than the sample limit introduces a systematic error in the estimate of the covariance matrix. However, if T_c is a few times larger than the measurable decay of $\xi_{XY}(t)$ (assuming ξ_{XY} falls exponentially for large enough t) the systematic error can be kept on the order of a few percent while leaving an estimator that has a variance which decreases in the large sample-size limit.

In this work, T_c has been determined as follows. The appropriate estimator for the error in $\xi_{XX}(t)$ is found by first calculating

$$\eta_{XXXX}(t,t',t'')=\frac{1}{N}\sum_i \hat{X}(t+t'+i)\hat{X}(t'+i)\hat{X}(t+t''+i) \times\hat{X}(t''+i) . \tag{26}$$

TABLE II. Integrated autocorrelation times for square loops.

Loop	$\beta=6.0$ Initial	$\beta=6.0$ Final	$\beta=10.0$ Initial	$\beta=10.0$ Final	$\beta=12.0$ Initial	$\beta=12.0$ Final
1×1	0.6	0.51	0.8	0.52	0.6	0.44
2×2	1.9	0.58	1.9	0.51	1.6	0.50
3×3	2.9	0.63	4.1	0.55	3.5	0.56
4×4	4.0	0.71	8.8	0.64	5.4	0.64
5×5	4.8	0.78	14.9	0.78	8.4	0.78
6×6	4.8	0.82	19.6	0.84	10.0	0.86
7×7	4.4	0.77	28.0	0.89	10.9	1.01
8×8	3.4	0.65	34.4	0.93	12.1	1.11
9×9	2.4	0.56	38.1	0.96	13.9	1.21
10×10	1.8	0.53	38.6	0.96	16.8	1.37
11×11	1.6	0.51	33.9	0.94	20.1	1.42
12×12	1.4	0.51	19.6	0.90	22.9	1.41
13×13	1.1	0.50	11.2	0.84	23.7	1.38
14×14	1.0	0.51	8.3	0.79	21.8	1.24
15×15	0.8	0.51	7.0	0.74	18.2	1.15
16×16	0.8	0.54	5.7	0.70	13.1	1.02

The variance of $\xi_{XX}(t)$ can be estimated from

$$\mathrm{var}\xi_{XX}(t)=\frac{1}{N^2}\sum_{t',t''}\eta_{XXXX}(t,t',t'')-\bar{\xi}^2_{XX}(t)\ . \qquad (27)$$

This sum must also be cut off and we use a cutoff which only includes terms with $t'=t''$. This just assumes that the dominant contribution comes when the terms cluster and that the true value should be larger than this estimate. This procedure gives a rough estimate of the variance $\xi_{XX}(t)$ and we use this to estimate where the signal in $\xi_{XX}(t)$ for large t falls into the noise. We call this value T_0. We then use the behavior of $\xi_{XX}(t)$ up to T_0 to determine an exponential decay constant τ_d for $\xi_{XX}(t)$ and take $T_c=4\tau_d$. This means we make a fractional systematic error of $\exp(-4)$ in our estimate of C_{XX}. When calculating the off-diagonal elements of the covariance matrix, we use as a cutoff the maximum of the two relevant T_c's.

The full covariance matrix is necessary to extract the value of $V(R)$. $V(R)$ can be found by fitting the negative logarithm of R by T Wilson loops to the function $aT+b$ for $T>R$ with fixed R. However, this simple linear form is only expected asymptotically and in order to judge whether the fits for any finite values are reasonable a reliable χ^2 is needed. If the Wilson loops are highly correlated (as they are in this simulation) a weighted least-squares fit with the full covariance matrix must be used to get a reliable χ^2. The quantity to be minimized by fitting is

$$\chi^2=\sum_{T_1,T_2}[-\ln W(R,T_1)-(aT_1+b)]C^{-1}_{-\ln W_1,-\ln W_2}$$
$$\times[-\ln W(R,T_2)-(aT_2+b)]\ . \qquad (28)$$

The covariance matrix for the logarithm of the Wilson loops can be easily gotten from the covariance matrix of the Wilson loops.

It is important to remember that we do not have the actual covariance matrix, but only an estimate of it. In particular we find that because of the strong correlation between loops whose dimensions differ by only a few lattice spacings, the estimator for the covariance matrix for the logarithm of the Wilson loops can have negative eigenvalues. This means that the χ^2 can be negative, which is clearly not desired. We chose to circumvent this problem by decorrelating our data slightly. To show how we do this, consider the Wilson loop averages for 5 by 5 and 6 by 6 loops. If we generate N lattices and measure both loops on all lattices, the results will be highly correlated. However, if we measure the 5 by 5 loops on the first $N/2$ lattices, and the 6 by 6 loops on the remaining lattices, the results will be completely decorrelated, although the standard deviations of the individual loops will be larger in the second method since there are only half as many measurements of each. Of course if the 5 by 5 loops are measured on the first $3N/4$ lattices and the 6 by 6 loops on the last $3N/4$ lattices, the results will be somewhat correlated.

We have solved the problem of negative eigenvalues of the covariance matrix in just this manner. We have not used all measurements of a given loop in the average, so that the average values obtained are somewhat decorrelated. (The number of measurements left out is 250 out of 5000 for $\beta=6.0$). After excluding some measurements the resulting covariance matrix is checked to see if it has any negative eigenvalues. In addition, the covariance matrix is also checked for negative eigenvalues when the off diagonal elements are randomly changed by 3–5%. (This is roughly the standard deviation of the covariance matrix elements for a sample of this size.) When the linear fits are done, the parameters and χ^2 are checked to make sure their dependence on small errors in the covariance matrix is small. [Because of the inverse appearing in (28), the computed χ^2 fluctuates wildly if an eigenvalue crosses through zero and becomes negative.]

Now that a reliable χ^2 has been calculated, one must still decide which T's are large enough that the asymptotic form is being reliably seen. Since the errors are becoming larger for large loops one would like to pick values for T which are bigger than R, but for which the statistics still give meaningful results. The values used for the potentials were determined from graphs such as Fig. 2 for each R. At fixed R, the logarithm of the Wilson loops was fit to a straight line from T to the maximum T measured (usually 16) and the uncertainty in the slope was calculated along with the χ^2. The χ^2 per degree of freedom (reduced χ^2) is also shown in Fig. 2. One generically sees the values of $V(R)$ level off when the reduced χ^2 enters the range 0.5–2.0 and this helps to determine which T to use. For the plot in Fig. 2 the value of $V(R)$ was chosen from the data point where $T=8$.

The errors for the Creutz ratios can also be calculated using the known covariance matrix, but a more reliable procedure, which does not require the subtraction of large numbers to get a small result, is binning. The measurements were broken into groups of 100 measurements each and the Creutz ratios were found for each group. The groups are now independent and the standard deviations can be easily calculated.

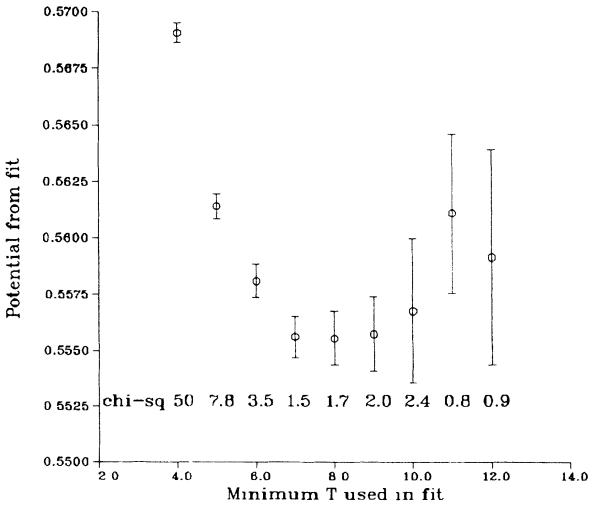

FIG. 2. Extracting the potential from linear fits to the logarithm of Wilson loops.

V. RESULTS

For an observable O, define $\langle O \rangle_1$ to be the expectation value of O using single variance reduction and $\langle O \rangle_2$ to be the expectation value with double variance reduction. Figure 3 is a graph of the ratios

$$\frac{\mathrm{var}\langle W_F(4,T)\rangle_1}{\mathrm{var}\langle W_F(4,T)\rangle_2} \tag{29}$$

and Fig. 4 is the same ratio for loops in the adjoint representation. The loops have had the reduction applied to all links on their T sides. The curves shown are from the estimates (19) and (21), which have been smoothly continued for noninteger numbers of links. In Fig. 3 the error bars have been suppressed for the loops at $\beta=10.0$ and 12.0 to increase legibility. These errors are very similar to the ones shown for the $\beta=6.0$ points.

One sees the greatest reduction in the variance of large loops at the smallest β. For the fundamental loops the asymptotic estimates of Sec. II are fairly good, although the errors for the data at $\beta=10.0$ and 12.0 are as large as the effect. From Fig. 4 one can see that the second reduction works noticeably better than the estimate for adjoint loops at $\beta=6.0$ and 10.0. Since the amount of variance reduction increases with more links, large loops will show larger improvements than the 4 by T loops in the graphs. The errors on the graphs were generated by first summing $\eta_{XXXX}(t,t',t'')$ over all $|t'-t''| \le T_c$. This gives the variance C_{XX} for the single and double reductions individually. The individual variances were then added and the square root of the sum taken to get the error shown in the graphs.

Table III shows the results for the scaled Creutz ratios $\beta^2 C(R,R)$ for both the adjoint and fundamental representations and Figs. 5 and 6 are a plot of these results. The data have been shifted along the abscissa of Figs. 5 and 6 to allow the error bars to be legibly included; all results

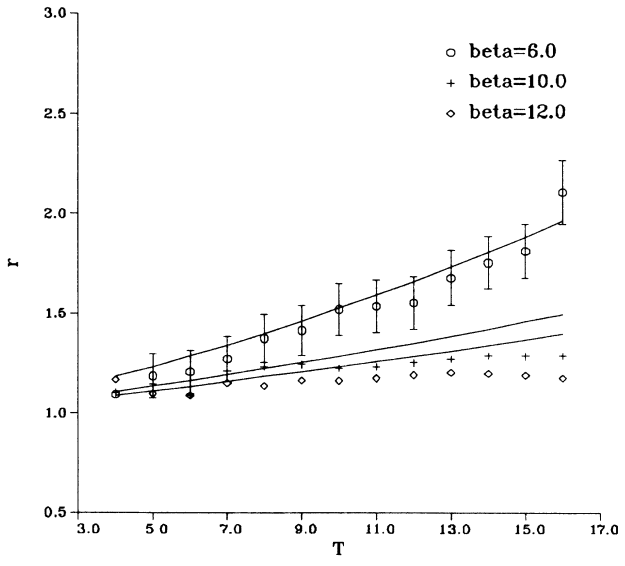

FIG. 3. The values of $r=\mathrm{var}\langle W_F(4,T)\rangle_1/\mathrm{var}\langle W_F(4,T)\rangle_2$.

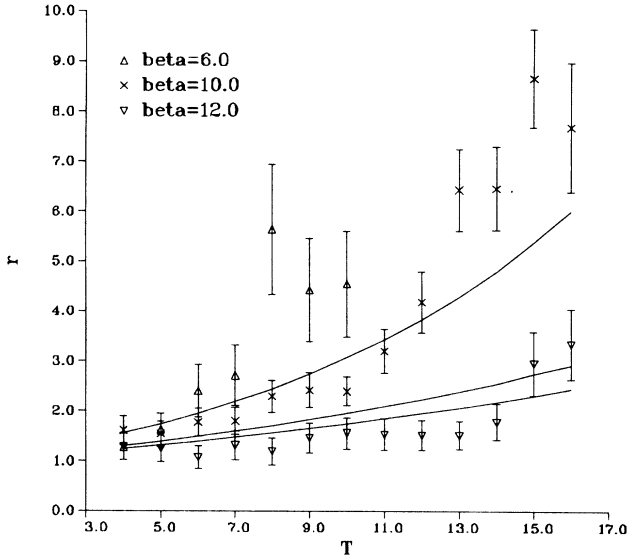

FIG. 4. The values of $r=\mathrm{var}\langle W_A(4,T)\rangle_1/\mathrm{var}\langle W_A(4,T)\rangle_2$.

are from $\beta=6.0$, 10.0, or 12.0. As mentioned, the errors come from breaking the measurements into groups of 100 and treating these groups as being statistically independent. The Creutz ratios for large loops are well converged and the large loop values are in good agreement with scaling. The adjoint loops show similar characteris-

TABLE III. Creutz ratios for the fundamental and adjoint representations.

R	$\beta=6.0$	$\beta=10.0$	$\beta=12.0$
		$\beta^2 C_F(R,R)$	
2	4.388 (1)	6.106 (1)	7.027 (2)
3	3.293 (2)	4.122 (3)	4.621 (3)
4	2.827 (5)	3.274 (6)	3.570 (9)
5	2.617 (5)	2.846 (5)	3.051 (4)
6	2.500 (9)	2.614 (7)	2.749 (7)
7	2.433 (18)	2.469 (10)	2.563 (11)
8	2.421 (53)	2.385 (13)	2.438 (13)
9	2.356 (144)	2.317 (20)	2.354 (18)
10	2.674 (610)	2.257 (34)	2.289 (26)
11		2.244 (47)	2.262 (30)
12		2.202 (67)	2.205 (44)
13		2.332 (150)	2.226 (67)
14		2.218 (300)	2.183 (120)
15			2.191 (190)
16			2.137 (260)
		$\beta^2 C_A(R,R)$	
3	8.68 (1)	10.99 (2)	12.33 (1)
4	7.34 (12)	8.69 (2)	9.50 (9)
5	6.81 (12)	7.52 (5)	8.17 (4)
6	7.54 (77)	6.82 (8)	7.38 (5)
7		6.30 (10)	6.83 (9)
8		6.35 (40)	6.94 (23)
9			6.55 (42)

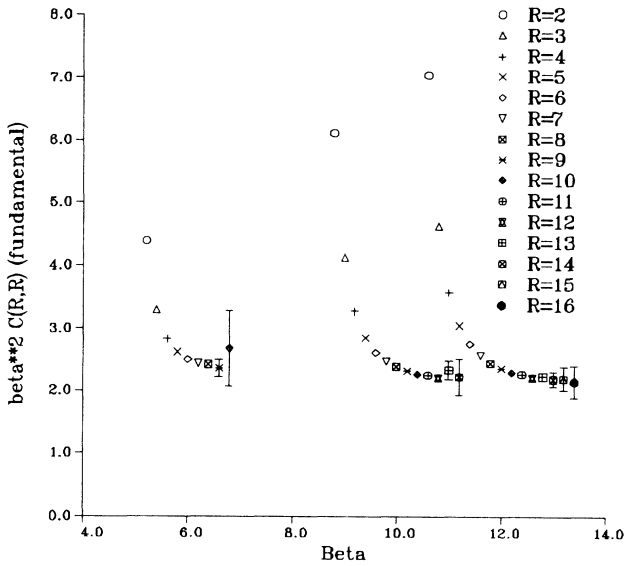

FIG. 5. The Creutz ratios for the fundamental representation, $\beta^2 C_F(R,R)$.

tics, although the statistics were worse.

Table IV gives the values for the potential for different R at each of the three β values. The errors are statistical, although a systematic error of about the size of the statistical errors could easily be present for the largest R's for each potential due to the ambiguity of extracting the true asymptotic form. The last column in the table gives the ratio of the adjoint potential to the fundamental potential for each of the different β's studied. One can easily see that the functional form of the potentials is extremely close and also that the ratio given is equal to the ratio of the Casimir operators for the two representations, 8/3. This has been seen previously in the string tensions[8] and is seen here to be the case for the potential as a whole. This is precisely the ratio predicted perturbatively, although here it clearly persists into the region where the potential is linear, as seen in Figs. 7 and 8.

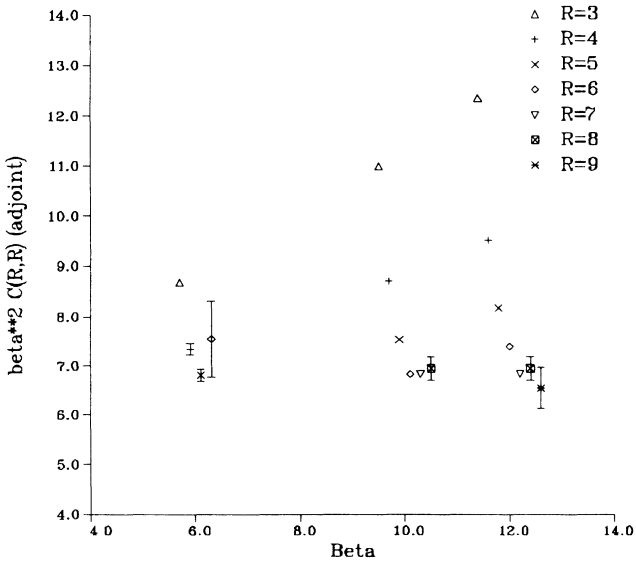

FIG. 6. The Creutz ratios for the adjoint representation, $\beta^2 C_A(R,R)$.

TABLE IV. Values of $V(R)$ for the fundamental and adjoint representations.

R	$V_F(R)$	$V_A(R)$	$V_A(R)/V_F(R)$
		$\beta=6.0$	
1	0.160 71 (5)	0.426 3 (9)	2.653 (6)
2	0.263 35 (8)	0.697 7 (8)	2.649 (3)
3	0.345 23 (27)	0.909 9 (40)	2.636 (12)
4	0.419 08 (32)	1.104 8 (33)	2.636 (8)
5	0.488 81 (62)	1.280 5 (111)	2.620 (23)
6	0.555 55 (120)	1.477 7 (200)	2.660 (36)
7	0.620 45 (303)	1.643 8 (430)	2.649 (70)
8	0.683 14 (588)		
9	0.752 78 (1184)		
10	0.750 87 (5503)		
		$\beta=10.0$	
1	0.086 34 (3)	0.230 5 (1)	2.670 (2)
2	0.134 10 (4)	0.357 3 (2)	2.664 (2)
3	0.168 38 (9)	0.448 1 (5)	2.661 (3)
4	0.196 94 (14)	0.523 8 (8)	2.660 (4)
5	0.222 82 (24)	0.592 7 (16)	2.660 (8)
6	0.246 85 (36)	0.652 6 (40)	2.664 (17)
7	0.270 84 (51)	0.721 1 (56)	2.662 (21)
8	0.293 67 (85)	0.773 7 (109)	2.635 (38)
9	0.316 20 (110)	0.821 1 (208)	2.597 (66)
10	0.337 94 (155)		
11	0.361 25 (236)		
12	0.381 76 (342)		
		$\beta=12.0$	
1	0.070 11 (2)	0.187 1 (2)	2.669 (3)
2	0.107 58 (3)	0.287 3 (3)	2.671 (2)
3	0.133 62 (8)	0.357 0 (4)	2.672 (3)
4	0.154 69 (13)	0.413 1 (8)	2.670 (6)
5	0.173 48 (21)	0.464 3 (13)	2.676 (8)
6	0.191 02 (31)	0.510 0 (22)	2.670 (12)
7	0.207 60 (42)	0.554 2 (34)	2.670 (17)
8	0.223 34 (67)	0.596 4 (114)	2.670 (52)
9	0.239 01 (87)	0.626 5 (93)	2.621 (40)
10	0.253 73 (136)	0.668 9 (193)	2.636 (77)
11	0.270 12 (169)	0.718 6 (702)	2.660 (260)
12	0.284 53 (224)		

The string tensions from fitting the potentials to a straight line for various ranges of R are given in Table V. A conventional weighted least-squares fit has been used here, since it would be extremely difficult to estimate the correlation between the values of the potential at different R's. (The smallness of the χ^2 for larger R's is an indication of correlations.) The errors given are statistical, but one can see systematic effects from fits to different ranges of R that are roughly twice the size of the statistical errors. The string tensions as determined from the potentials have similar statistical errors to those determined from the Creutz ratios. However, since the string ten-

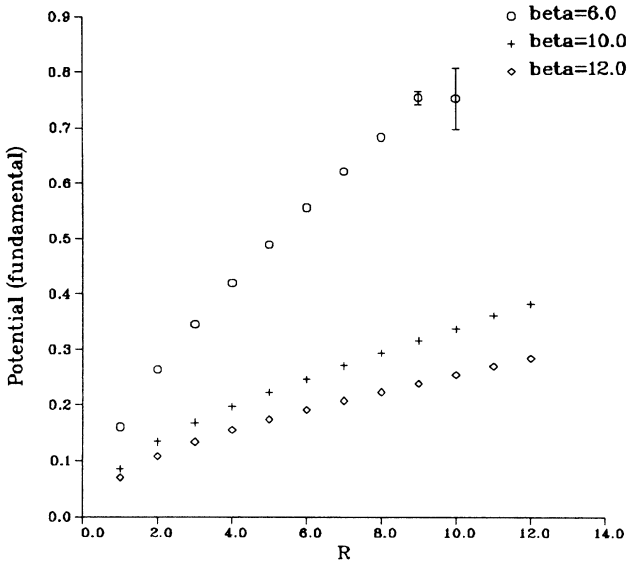

FIG. 7. The potential for the fundamental representation.

TABLE V. Fundamental- and adjoint-representation string tensions from fits to the potentials.

β	Range of R	$\beta^2\sigma_F$	χ^2
6.0	4–10	2.458 (15)	2.2
6.0	5–10	2.373 (33)	0.6
6.0	6–10	2.316 (72)	0.5
6.0	7–10	2.282 (166)	0.7
10.0	5–12	2.340 (14)	1.9
10.0	6–12	2.298 (22)	0.9
10.0	7–12	2.247 (33)	0.1
12.0	5–12	2.362 (17)	3.7
12.0	6–12	2.283 (25)	0.7
12.0	7–12	2.235 (37)	0.1
12.0	8–12	2.216 (59)	0.1
β	Range of R	$\beta^2\sigma_A$	χ^2
6.0	4–7	6.53 (25)	0.3
10.0	4–9	6.55 (10)	1.9
10.0	5–9	6.15 (20)	0.6
10.0	6–9	6.13 (42)	1.0
12.0	5–11	6.26 (18)	0.7
12.0	6–11	5.88 (32)	0.4
12.0	7–11	5.40 (56)	0.1

sions extracted from the potentials involve two asymptotic fits to straight lines, they are subject to systematic errors.

Figure 9 is a plot of $\beta^2 V_F(R)$ and $\frac{3}{8}\beta^2 V_A(R)$ for each of the couplings used. The very similar functional form of the fundamental and adjoint potentials is evident. The visual evidence for scaling is quite strong as can be seen by the similar slopes for large R for each of the different β's.

Table VI gives a single result for the string tension at each β, where the errors reflect an estimate of the range in which the true value should lie. This estimated error covers the range of results from both the Creutz ratios and the potentials.

In Ref. 2 the authors have used a simple string model to argue that Wilson loops with $T > R$ could be expected to behave (for β greater than about 3.0) as

$$-\ln W(R,T)=\theta_1(\beta)RT+\theta_2(\beta)(R+T)-\theta_3(\beta)T/R - \theta_4(\beta)\ln R+\theta_5(\beta)\ , \tag{30}$$

where the θ's are parameters. $\theta_1(\beta)$ is the string tension and $\theta_3(\beta)$ is expected to be $\pi/24$, the coefficient of the

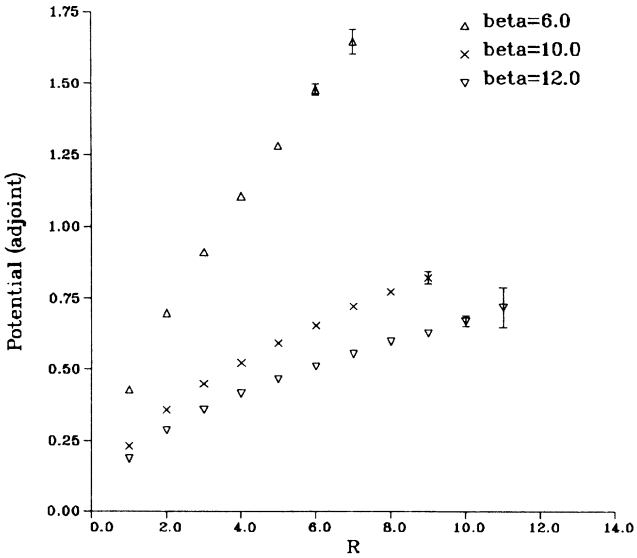

FIG. 8. The potential for the adjoint representation.

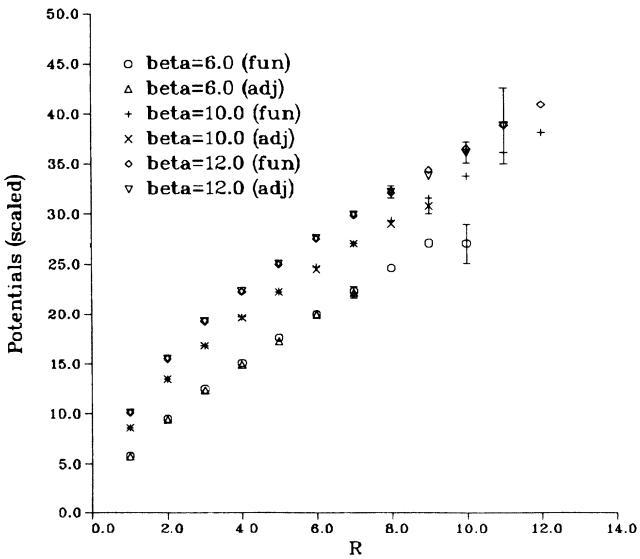

FIG. 9. The scaled potentials $\beta^2 V_F(R)$ and $(3/8)\beta^2 V_A(R,R)$.

TABLE VI. Final results for the fundamental- and adjoint-representation string tensions.

β	$\beta^2\sigma_F$
6.0	2.35 (8)
10.0	2.25 (4)
12.0	2.23 (4)
β	$\beta^2\sigma_A$
6.0	6.7 (3)
10.0	6.2 (2)
12.0	6.2 (7)

universal Coulomb potential. They find that the form (30) well represents their data.

An advantage of using fitting to (30) is that many of the loops measured at a given β are used simultaneously to determine the string tension, with a resulting decrease in the statistical errors. However, there are difficulties in using (30) to extract the string tension and other θ's. The main problem is the high correlation between the measured loops. We find that the covariance matrix for almost all groups of loops has negative eigenvalues and moderate decorrelating as discussed in Sec. IV is inadequate to cure the problem. (The loops can always be fully decorrelated by measuring one size loop on the first 100 lattices, another on the second 100, etc., but the errors for the individual loops would increase enormously.) If one proceeds and neglects correlations, the resulting statistical errors on the θ's are extremely small (as small as 0.2%), while the values of the θ's are only stable to a few percent when the range of fitting is varied. (Our $\beta=6.0$ results are in agreement with Ref. 2.) Without a reliable χ^2 there is no criteria for determining which range for R and T to use, nor how good the fits are. Hence, it appears that although (30) is a good representation of the general form of the Wilson loops, it is difficult to make this statement exact or take advantage of the reduced statistical error from such a fit.

VI. CONCLUSIONS

We have done an updated simulation of $SU(2)_3$ and have seen a scaling string tension in both the fundamental and adjoint representations. The fundamental representation string tension shows deviations from scaling of at most a few percent. Our results are in agreement with earlier studies done for $\beta=6.0$, which is the only coupling in common. We find the functional form of the potentials for the fundamental and adjoint representations is the same to high accuracy.

We have seen no sign of the expected departure of the adjoint potential from linearity at large R. This is reasonable as seen by using the mass values from Ref. 3. There the mass is given as $8.6/\beta$, so the value of R needed to have enough energy in the string to form two glueballs is

$$R\frac{2.2}{\beta^2}\sim 2\frac{8.6}{\beta}\ , \tag{31}$$

$$R\sim 8\beta\ . \tag{32}$$

At this value the string would be completely broken and it is not surprising that no trace of this is seen for R's eight times smaller.

The double variance reduction has improved the statistics for 4 by T loops by up to a factor of ~ 3 (for the 4 by 16 loop in the adjoint representation at $\beta=10.0$). Larger loops should show even greater reduction, although we have not explicitly measured the reduction. This reduction costs only slightly more computer time, although it does increase the complexity of the measurement algorithm substantially. Although not a long simulation by current standards, the 80 h of Cray-XMP time used would have gone up by at least a factor of 10 without the second variance reduction, if comparable statistics were desired.

At fixed β, the peak in the autocorrelation times for loops of size β by β is an unexpected and interesting result. One possible explanation for this peak is the existence of field configurations on the lattice of roughly volume β^3 which have structure which the heat-bath algorithm cannot easily modify. We are currently investigating this possibility.

ACKNOWLEDGMENTS

The author gratefully acknowledges a grant from the Pittsburgh Supercomputing Center which allowed this work to be done. In addition the author would like to thank Claudio Rebbi, Ralph Roskies, and particularly Tony Duncan for helpful discussions and comments and Kevin Cahill for his (then) unpublished data on this model.[9] This work was supported in part by NSF Grant No. PHY-87-20221.

[1]P. de Forcrand, J. Stat. Phys. **43**, 1077 (1986); C. Rebbi, *ibid.* **43**, 1117 (1986).

[2]J. Ambjorn, P. Olesen, and C. Peterson, Nucl. Phys. **B244**, 262 (1984).

[3]A. Irback and C. Peterson, Phys. Lett. B **174**, 99 (1986); K. Farakos, G. Koutsoumbas, and S. Sarantakos, *ibid.* **189**, 173 (1987).

[4]G. 't Hooft, Nucl. Phys. **B138**, 1 (1978); R. P. Feynman, *ibid.* **B153**, 141 (1979); R. D. Mawhinney, *ibid.* **B321**, 653 (1989).

[5]G. Parisi, R. Petronzio, and F. Rapuano, Phys. Lett. **126B**, 250 (1983).

[6]J. Ambjorn, A. J. G. Hey, and S. Otto, Nucl. Phys. **B210** [FS6], 347 (1982).

[7]N. Madras and A. D. Sokal, J. Stat. Phys. **50**, 109 (1988).

[8]J. Ambjorn, P. Olesen, and C. Peterson, Nucl. Phys. **B240** [FS12], 533 (1984).

[9]K. Cahill and S. Prasad, Phys. Rev. D **40**, 1274 (1989).